Frequency tunable near-infrared metamaterials based on VO_2 phase transition

Matthew J. Dicken[1*‡], Koray Aydin[1*], Imogen M. Pryce[1*], Luke A. Sweatlock[2], Elizabeth M. Boyd[1], Sameer Walavalkar[1], James Ma[2], and Harry A. Atwater[1†]

[1] *California Institute of Technology, 1200 E. California Boulevard, Pasadena, California, USA*
[2] *Northrop Grumman Aerospace Systems, One Space Park, Redondo Beach, California, USA*
[†] *haa@caltech.edu*

Abstract: Engineering metamaterials with tunable resonances from mid-infrared to near-infrared wavelengths could have far-reaching consequences for chip based optical devices, active filters, modulators, and sensors. Utilizing the metal-insulator phase transition in vanadium oxide (VO_2), we demonstrate frequency-tunable metamaterials in the near-IR range, from 1.5 - 5 microns. Arrays of Ag split ring resonators (SRRs) are patterned with e-beam lithography onto planar VO_2 and etched via reactive ion etching to yield Ag/VO_2 hybrid SRRs. FTIR reflection data and FDTD simulation results show the resonant peak position red shifts upon heating above the phase transition temperature. We also show that, by including coupling elements in the design of these hybrid Ag/VO_2 bi-layer structures, we can achieve resonant peak position tuning of up to 110 nm.

OCIS codes: (160.3918) Metamaterials; (310.6845) Thin film devices and applications

References and links

1. V. M. Shalaev, "Optical negative-index metamaterials," Nat. Photonics **1**(1), 41–48 (2007).
2. D. R. Smith, J. B. Pendry, and M. C. K. Wiltshire, "Metamaterials and negative refractive index," Science **305**(5685), 788–792 (2004).
3. V. G. Veselago, "The electrodynamics of substances with simultaneously negative values of permittivity and permeability," Sov. Phys. Usp. **10**, 504–509 (1968).
4. S. Linden, C. Enkrich, M. Wegener, J. F. Zhou, T. Koschny, and C. M. Soukoulis, "Magnetic response of metamaterials at 100 terahertz," Science **306**(5700), 1351–1353 (2004).
5. T. J. Yen, W. J. Padilla, N. Fang, D. C. Vier, D. R. Smith, J. B. Pendry, D. N. Basov, and X. Zhang, "Terahertz magnetic response from artificial materials," Science **303**(5663), 1494–1496 (2004).
6. G. Dolling, M. Wegener, C. M. Soukoulis, and S. Linden, "Negative-index metamaterial at 780 nm wavelength," Opt. Lett. **32**(1), 53–55 (2007).
7. V. M. Shalaev, W. S. Cai, U. K. Chettiar, H. K. Yuan, A. K. Sarychev, V. P. Drachev, and A. V. Kildishev, "Negative index of refraction in optical metamaterials," Opt. Lett. **30**(24), 3356–3358 (2005).
8. R. A. Shelby, D. R. Smith, and S. Schultz, "Experimental verification of a negative index of refraction," Science **292**(5514), 77–79 (2001).
9. J. Valentine, S. Zhang, T. Zentgraf, E. Ulin-Avila, D. A. Genov, G. Bartal, and X. Zhang, "Three-dimensional optical metamaterial with a negative refractive index," Nature **455**(7211), 376–379 (2008).
10. J. B. Pendry, "Negative refraction makes a perfect lens," Phys. Rev. Lett. **85**(18), 3966–3969 (2000).
11. X. Zhang, and Z. Liu, "Superlenses to overcome the diffraction limit," Nat. Mater. **7**(6), 435–441 (2008).
12. W. S. Cai, U. K. Chettiar, A. V. Kildishev, and V. M. Shalaev, "Optical cloaking with metamaterials," Nat. Photonics **1**(4), 224–227 (2007).
13. J. B. Pendry, D. Schurig, and D. R. Smith, "Controlling electromagnetic fields," Science **312**(5781), 1780–1782 (2006).
14. D. Schurig, J. J. Mock, B. J. Justice, S. A. Cummer, J. B. Pendry, A. F. Starr, and D. R. Smith, "Metamaterial electromagnetic cloak at microwave frequencies," Science **314**(5801), 977–980 (2006).
15. H. T. Chen, W. J. Padilla, J. M. O. Zide, A. C. Gossard, A. J. Taylor, and R. D. Averitt, "Active terahertz metamaterial devices," Nature **444**(7119), 597–600 (2006).
16. H.-T. Chen, W. J. Padilla, M. J. Cich, A. K. Azad, R. D. Averitt, and A. J. Taylor, "A metamaterial solid- state terahertz phase modulator," Nat. Photonics **3**(3), 148–151 (2009).
17. H.-T. Chen, J. F. O'Hara, A. K. Azad, A. J. Taylor, R. D. Averitt, D. B. Shrekenhamer, and W. J. Padilla, "Experimental demonstration of frequency-agile terahertz metamaterials," Nat. Photonics **2**(5), 295–298 (2008).

#115088 - $15.00 USD Received 11 Aug 2009; revised 17 Sep 2009; accepted 18 Sep 2009; published 25 Sep 2009

18. T. Driscoll, S. Palit, M. M. Qazilbash, M. Brehm, F. Keilmann, B. G. Chae, S. J. Yun, H. T. Kim, S. Y. Cho, N. M. Jokerst, D. R. Smith, and D. N. Basov, "Dynamic tunig of an infrared hybrid-metamaterial resonance using vanadium dioxide," Appl. Phys. Lett. **93**(2), 024101 (2008).
19. J. B. Goodenough, "The two components of crystallographic transition in VO2," J. Solid State Chem. **3**(4), 490–500 (1971).
20. F. J. Morin, "Oxides which show a metal-to-insulator transition at the Neel temperature," Phys. Rev. Lett. **3**(1), 34–36 (1959).
21. A. Cavalleri, T. Dekorsy, H. H. W. Chong, J. C. Kieffer, and R. W. Schoenlein, "Evidence for a structurally-driven insulator-to-metal transition in VO_2: A view from the ultrafest timescale," Phys. Rev. B **70**(16), 161102 (2004).
22. A. Cavalleri, C. Tóth, C. W. Siders, J. A. Squier, F. Ráksi, P. Forget, and J. C. Kieffer, "Femtosecond structural dynamics in VO2 during an ultrafast solid-solid phase transition," Phys. Rev. Lett. **87**(23), 237401 (2001).
23. G. Stefanovich, A. Pergament, and D. Stefanovich, "Electrical switching and Mott transition in VO_2," J. Phys. Condens. Matter **12**(41), 8837–8845 (2000).
24. R. Lopez, L. C. Feldman, and R. F. Haglund, Jr., "Size-dependent optical properties of VO_2 nanoparticle arrays," Phys. Rev. Lett. **93**(17), 177403 (2004).
25. E. U. Donev, R. Lopez, L. C. Feldman, and R. F. Haglund, "Confocal Raman microscopy across the metal-insulator transition of single vanadium dioxide nanoparticles," Nano Lett. **9**(2), 702–706 (2009).
26. J. Y. Suh, E. U. Donev, R. Lopez, L. C. Feldman, and R. F. Haglund, "Modulated optical transmission of subwavelength hole arrays in metal-VO2 hole films," Appl. Phys. Lett. **88**(13), 133115 (2006).
27. M. M. Qazilbash, M. Brehm, B. G. Chae, P. C. Ho, G. O. Andreev, B. J. Kim, S. J. Yun, A. V. Balatsky, M. B. Maple, F. Keilmann, H. T. Kim, and D. N. Basov, "Mott transition in VO2 revealed by infrared spectroscopy and nano-imaging," Science **318**(5857), 1750–1753 (2007).
28. V. A. Fedotov, M. Rose, S. L. Prosvirnin, N. Papasimakis, and N. I. Zheludev, "Sharp trapped-mode resonances in planar metamaterials with a broken structural symmetry," Phys. Rev. Lett. **99**(14), 147401 (2007).
29. H. C. Guo, N. Liu, L. Fu, T. P. Meyrath, T. Zentgraf, H. Schweizer, and H. Giessen, "Resonance hybridization in double split-ring resonator metamaterials," Opt. Express **15**(19), 12095–12101 (2007).

1. Introduction

Electromagnetic resonances in subwavelength metallic resonators can be used to engineer optical responses not found in natural materials [1,2]. Metamaterials have reemerged following their initial introduction [3], and are the subject of intensive investigation for applications in frequency selective surfaces [4,5] and transformation optics, e.g. negative-index materials [6–9], super-lensing [10,11], and cloaking [12–14]. Active metamaterials have been demonstrated at terahertz frequencies using carrier depletion in GaAs [15,16], photoexcitation of free charge carries in Si [17], and the metal-insulator phase transition in vanadium oxide thin films [18]. Typical metamaterials consist of arrays of metal structures embedded in a dielectric with feature sizes much smaller than the desired operating wavelength. In the simplest sense, the unit cell of a metamaterial array is designed to be an individual "LC" circuit with resonant frequency, $\omega_o \sim (LC)^{-1/2}$ [4]. Split-ring resonators (SRRs) are the basis for many metamaterial designs due to ease of fabrication and modeling. Each SRR has a distributed inductance, L, and a distributed capacitance, C, arising from charge build-up at the notch. The choice of materials and the resonator dimensions set these two parameters and determine the resonant frequency of the metamaterial. Active metamaterial designs have previously focused on changing the capacitance in the SRR gap to modulate the amplitude of the resonance [15–17]. Integrating materials with tunable electrical or optical properties allows further control over the resonant response in metamaterials. Vanadium oxide is a promising candidate that exhibits a dramatic change in its complex refractive index arising from a structural phase transition from monoclinic to rutile. Here, we propose an alternative geometry consisting of self-aligned, hybrid Ag/VO_2 SRR bi-layers as an approach to tuning the metamaterial response in the near-IR by controlling the resonator geometry with the phase transition. VO_2 undergoes a structural transition from an insulating monoclinic phase to a metallic rutile phase at 68 °C [19,20]. This phase transition can occur on a sub-picosecond timescale [21] and can be induced thermally, optically [22] or electrically [23]. As a result of the insulator-to-metal transition, the conductivity increases by as much as four orders of magnitude and the optical transmission in the near-IR decreases significantly [24]. Drastic changes in the optical properties of VO_2 with the phase transition enable control over

#115088 - $15.00 USD Received 11 Aug 2009; revised 17 Sep 2009; accepted 18 Sep 2009; published 25 Sep 2009

the transmission and reflection properties of nanophotonic structures, such as nanoparticles [24,25], hole arrays [26], and metamaterials [18].

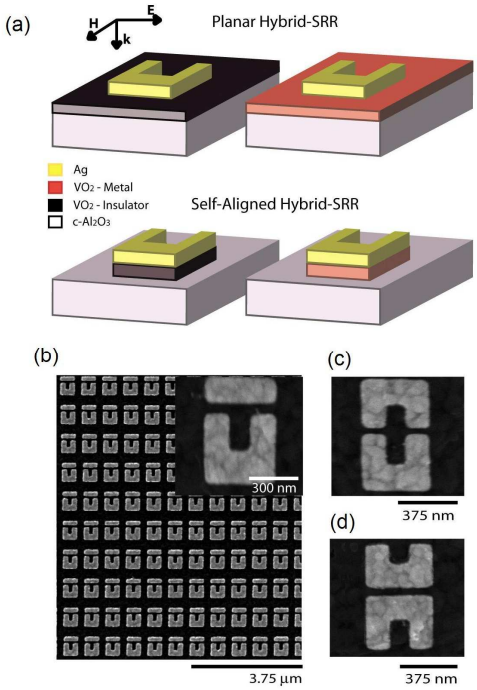

Fig. 1. Hybrid split-ring resonator metamaterials based on vanadium oxide. (a) Schematic of a self-aligned silver/vanadium oxide metamaterial unit cell. The 150 nm thick silver SRR is fabricated by e-beam patterning and metal lift-off. 70 X 70 µm arrays of these structures sit on 60 nm of VO_2. A 10 nm chromium mask protects the silver SRR during etching. (b-d) SEM images of the three coupled-SRR metamaterial arrays studied in this work. These designs yield multiple resonances in the near-IR spectrum.

2. Ag/VO_2 active metamaterials: simulations and experiments

2.1 Unit cell design

The active metamaterial device design presented here consists of self-aligned Ag/VO_2 SRR arrays (Fig. 1a). The VO_2 thin films are grown epitaxially by pulsed laser deposition on c-plane Al_2O_3 substrates at 500 °C. A vanadium metal target is used as the source material and deposition takes place in 12 mTorr oxygen. 60 nm thick VO_2 films are deposited with a 300 mJ laser pulse at a rate of 10 Hz. Utilizing the insulator-metal phase transition in VO_2, we can control the effective dimensions of the unit cell as well as the optical properties of the hybrid-SRR arrays in both phases. Coupled asymmetric split-ring resonators are employed to reduce the spectral linewidth at the resonance frequency (Fig. 1b-d). A narrower resonant peak will increase the tuning figure of merit (FOM), the ratio of the tuning range to the full width at half maximum (FWHM) of the resonant peak. In this work, we investigate four self-aligned hybrid-SRR structures including two coupled SRR systems and one SRR coupled to a nanowire.

#115088 - $15.00 USD Received 11 Aug 2009; revised 17 Sep 2009; accepted 18 Sep 2009; published 25 Sep 2009

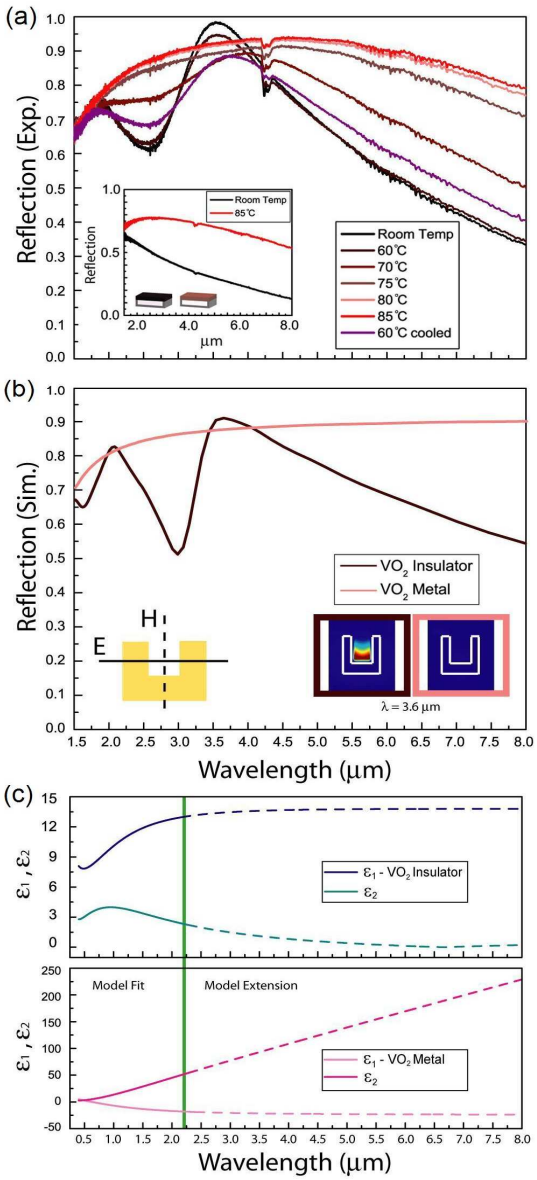

Fig. 2. (a). Near-IR reflection spectra of 150 nm thick Ag metamaterial arrays on 60 nm VO_2 thin films. As the temperature is increased above the insulator-metal transition temperature of VO_2, the near-IR spectral reflection properties of the SRR array become similar to those of a non-patterned metal-phase VO_2 film (inset). (b) Simulated reflection spectra for the same structure using FDTD. Magnetic field intensity, $|H_z|^2$ plots at the resonant peak position, show the resonance disappear as the structures become electrically shorted by the metal-phase VO_2 (inset). (c) Variable angle spectroscopic ellipsometry is used to model the complex optical constants of VO_2 thin films. Multi-oscillator ellipsometric models were used to extrapolate to the near and mid-IR to aid in FDTD simulations.

2.2 Active Ag SRR arrays on planar VO_2 substrates

The metamaterial arrays are fabricated on a 60 nm thick planar VO_2 film using standard electron beam lithography and evaporation of 150 nm of silver and 10 nm of chromium to act as an etch mask. SRR arrays are tested using the reflection mode of an FTIR microscope

#115088 - $15.00 USD Received 11 Aug 2009; revised 17 Sep 2009; accepted 18 Sep 2009; published 25 Sep 2009

using a light source in the range of 1.5 – 8 microns. Reflection data were normalized using an optically thick gold standard. Electromagnetic radiation, normally incident to the SRR array (along the *z*-direction) with the incident E-field polarized perpendicular to the SRR arms, was used to efficiently couple to the resonators and induce circulating currents in the structures (Fig. 1a). Two resonant reflection peaks, 2.1 μm (electric resonance) and 3.6 μm (magnetic "LC" resonance), were observed as shown in Fig. 2a. The sample was subsequently heated to temperatures above the insulator-metal phase transition temperature and then cooled using a commercial heating stage comprised of a silver block with a tiny aperture milled in the center. The resulting spectra show a continuous change from two distinct metamaterial resonant peaks to a broad reflection indicative of metallic VO_2. Although there is a slight hysteresis, the resonances are recovered upon cooling below the phase transition temperature. We also measured the reflection from a 60 nm thick VO_2 film on sapphire substrate at room temperature and 85 °C. The reflection intensity at 3.6 μm increased from 0.36 to 0.75, indicating a drastic change in complex refractive index of the VO_2 thin film upon phase change (Inset of Fig. 2a).

The resonant response was modeled using Lumerical, a commercially available finite-difference time-domain (FDTD) simulation software. A unit cell of the investigated structure is simulated using periodic boundary conditions along the *x* and *y* axes and perfectly matched layers along the axis of propagation of the electromagnetic waves (*z* axis). A broadband plane wave is incident on the unit cell along + *z* direction, and reflection is monitored by a power monitor that is placed behind the radiation source. Electric and magnetic fields are monitored by frequency profile monitors. Figure 2b shows the simulated response of an Ag SRR array on a planar VO_2 thin film in both the insulator and metallic phases. To accurately simulate the metamaterial response, we measured the complex refractive index of the VO_2 thin films in both phases (Fig. 2c) using variable angle spectroscopic ellipsometry. In the insulator phase, the VO_2 optical constants are fit to a Tauc-Lorentz model. In the metal phase, VO_2 acts like a Drude metal with strong absorption. These models were used to extrapolate the results to the near and mid-IR to aid in FDTD simulations. The simulated reflection spectra in both VO_2 phases agree well with the measured data.

We calculated the magnetic field intensity, $|H_z|^2$ at λ = 3.6 μm (inset of Fig. 2b) for the SRR array in the insulator (right) and metallic phases (left) of VO_2. The resonant behavior in the insulator phase is evident from the magnetic field profile, in which the magnetic field is concentrated at the center of SRR due to the excitation of circular surface currents at the resonance frequency. However, in the metallic VO_2 phase the LC circuit of each SRR is shorted and the array no longer resonates. Although the resonant behavior of the metamaterial can be switched with the phase transition of a VO_2 thin film, this switch is essentially bimodal. In the metallic phase the sample is highly reflecting and behaves like a mirror at IR wavelengths, meaning that the spectral selectivity required for practical applications is not achieved. To overcome this problem, we propose a self-aligned SRR design composed of a stack of Ag and VO_2 layers, whose resonant frequency could be modulated thermally.

2.3 Active Ag/VO_2 hybrid-SRR metamaterials

The samples are etched using reactive ion etching to yield self-aligned hybrid-SRR arrays. The 100 Watt CF_4/O_2 plasma etches the VO_2 film not masked by the Cr/Ag SRR structures to yield hybrid Ag/VO_2 SRR elements. Figure 3a shows experimental reflection spectra for self-aligned Ag/VO_2 SRR structures with dimensions of 450 × 400 nm and 150 nm width SRR arms (inset). The resonant reflection peak is observed at 2.52 μm, compared to 3.6 μm before etching. The blue shifting of the metamaterial resonance is a direct effect of replacing much of the underlying high dielectric constant VO_2 substrate with air. Upon heating above the insulator-metal phase transition temperature to 100 °C, the resonant reflection response of the new hybrid-SRR structure red shifts by $\Delta\lambda$ = 100 nm to 2.62 μm. A schematic of the self-aligned hybrid-SRR unit cell is shown in Fig. 1a.

#115088 - $15.00 USD Received 11 Aug 2009; revised 17 Sep 2009; accepted 18 Sep 2009; published 25 Sep 2009

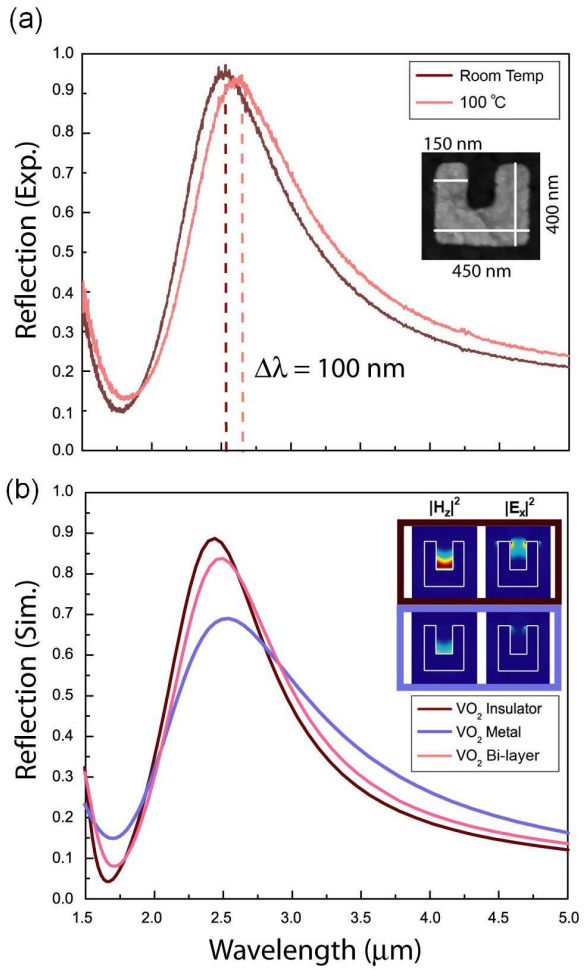

Fig. 3. Active self-aligned hybrid-SRR arrays. (a) Near-IR reflection spectra of self-aligned 150 nm Ag / 60 nm VO_2 hybrid-SRR arrays. The magnetic resonant peak shifts by 100 nm upon heating as the VO_2 undergoes a phase transition. (b) FDTD simulations of the self-aligned hybrid-SRR array. Simulations show a resonant peak shift of the same magnitude as experiment. A bi-layer VO_2 model (15 nm thick metal phase, 45 nm thick insulator phase) is used to predict the experimental results (Inset) Simulated field intensity profiles ($|H_z|^2$, and $|E_x|^2$) at $\lambda = 2.5$ μm for hybrid metamaterials show resonances both for insulating and metallic VO_2 phases.

Simulations of the metamaterial array show a similar red shift (≈100 nm) with an associated overall decrease in the reflection due to the increased absorption in the VO_2 metallic phase (Fig. 3b, blue line). However, this initial simulation result does not agree well with the measurements, in which the reflection peak intensity is not drastically reduced. Additional simulations were performed to investigate the behavior observed in the experiment. The experimental results suggest that the nanostructured VO_2 is not a homogeneous metallic rutile phase, but represents a nanocomposite phase where the semiconductor and metallic phases co-exist. Other researchers have reported that the VO_2 phase transition occurs via nanoscale domain switching rather than a bulk homogeneous phase transformation [27], and the phase transition and optical properties of nanoscale VO_2 structures have been shown to differ from those seen in continuous thin films [24]. Given that the actual switching mechanism is likely inhomogeneous for patterned nanoscale structures,

#115088 - $15.00 USD Received 11 Aug 2009; revised 17 Sep 2009; accepted 18 Sep 2009; published 25 Sep 2009

and that characterization of the actual domain structure is non-trivial, we employed the simplest model possible that provides good quantitative agreement with experimental observations: we assume that the heated 60 nm thick VO_2 film is a bilayer composed of a 15 nm thick VO_2 film in the metallic phase at the Ag/VO_2 interface and a 45 nm thick VO_2 film in the semiconductor phase at the VO_2/sapphire interface (Fig. 3b, light red line). The increase in peak intensity for the bilayer model approaches to that of observed in the experimental data. Based on the experiments and simulations, we conclude that the optical thickness of the VO_2 layer is different than the geometric thickness. It is also important to note that the optical properties of VO_2 films in both phases were measured up to 2.2 μm, above which we extrapolated the complex refractive index data by fitting to the ellipsometric models as shown in Fig. 2c.

Simulated magnetic and electric field intensity plots ($|H_z|^2$, and $|E_x|^2$) of the self-aligned SRR structure (λ = 2.5 μm) for both the insulator and metallic VO_2 phases are shown as insets in Fig. 3b. The resonant behavior is evident in the field profiles. At the resonant wavelengths, the electric field is strongly localized between the edges of the SRR arms due to the circular currents on the SRR. Since VO_2 has higher losses in the metallic phase, the calculated intensities of the magnetic and electric fields are lower compared to those in the insulator phase. When the active material is in the insulator phase, each unit cell of the metamaterial array acts as a 150 nm thick Ag SRR on a 60 nm thick VO_2 substrate. Upon heating above the phase transition temperature, the effective optical thickness of the resonator element changes due to the phase transition which causes the effective capacitance and inductance of the SRR element to increase and the resonant frequency to decrease. The proposed hybrid metal/VO_2 design is applicable to any resonator element in which the resonant behavior depends on the effective optical thickness.

2.4 Active coupled asymmetric Ag/VO_2 hybrid-SRR metamaterials

Frequency selective metamaterial surfaces could be used as modulators, filters and sensors at IR wavelengths. For practical applications, it is desirable to tune the resonant wavelength by a line-width of the resonance peak (FWHM). As seen in Fig. 3a, the resonance line-width of an ordinary SRR array is fairly broad (FWHM ≈1.25 μm) and $\Delta\lambda$ ≈100 nm tuning is relatively small compared to the resonance bandwidth. In order to increase the FOM, the ratio of $\Delta\lambda$ to the FWHM of the resonant peak, one could either increase the wavelength tuning range ($\Delta\lambda$) or decrease the line width of the resonance. Here, we demonstrate spectral line width narrowing of metamaterial resonances by introducing coupled asymmetric SRRs at near-IR wavelengths.

Figure 4 shows the experimental reflection spectra for coupled, self-aligned, Ag/VO_2 hybrid-SRR structures in the near-IR range from 1.5 – 5.0 microns. First, a SRR structure coupled to a nearby nanowire (Fig. 1b) is investigated in Fig. 4a. We observe two resonant reflection peaks, λ_1 and λ_2, that can be attributed to electrical and magnetic resonances, respectively. Magnetic and electric field intensities in the insulator phase are plotted in the inset. The reflection peak at λ_1 = 1.8 μm is due to the electric dipole resonance of the nanowire. The magnetic fields are localized around the nanowire due to the surface current flowing parallel the nanowire. At the electric dipole resonance wavelength, simulations predict strong localization of electric fields at the ends of the nanowire. The resonant wavelength, λ_1, does not change when the VO_2 switches phase. The wavelength of the nanowire dipole electric resonance is determined by the nanowire length and does not depend significantly on the thickness of the metal.

#115088 - $15.00 USD Received 11 Aug 2009; revised 17 Sep 2009; accepted 18 Sep 2009; published 25 Sep 2009

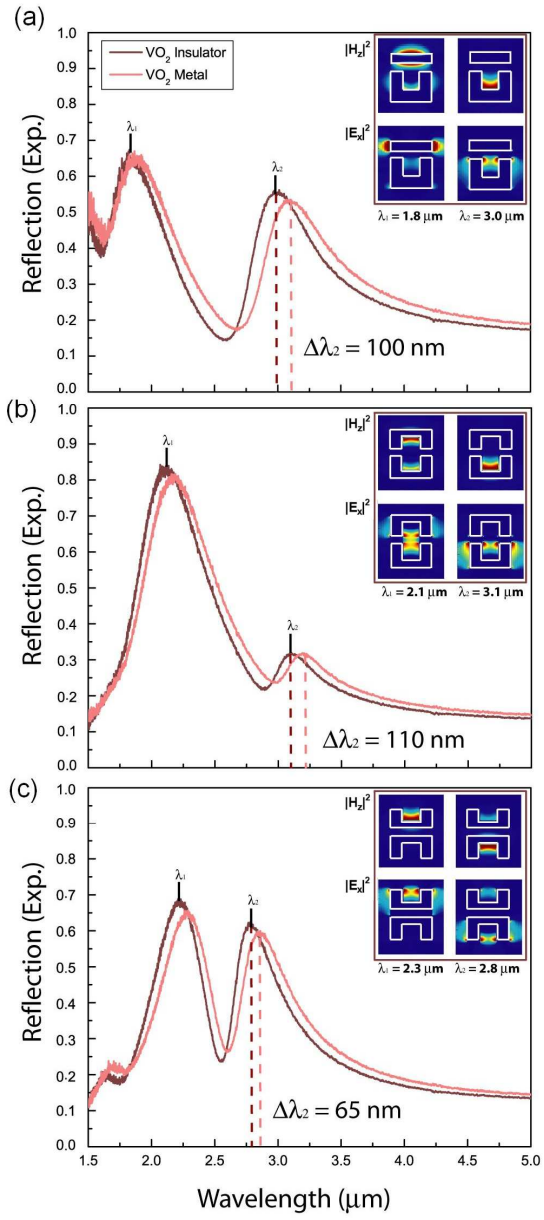

Fig. 4. Active coupled asymmetric Ag/VO_2 hybrid-SRR metamaterials (a) Electric and magnetic resonances are seen in the SRR coupled to a bar. The magnetic resonance at 3.0 μm shifted by 100 nm to 3.1 μm. Simulated field plots (inset) at the resonant wavelengths show $|H_z|^2$ (top) and $|E_x|^2$ (bottom) of the self-aligned structures on insulating VO_2. (b) Face-to-face coupled structures show an enhanced resonance at the shorter wavelength, λ_1 = 2.1 μm, and decreased reflection resonance at λ_2 = 3.1 μm. (c) Back-to-back coupled structures have magnetic resonant reflection peaks at λ_1 = 2.3 μm and λ_2 = 2.8 μm which shift by 65 nm upon VO_2 switching.

The resonant peak at the higher wavelength, λ_2 = 3.0 μm, is due to the magnetic resonance, as evident by the characteristic magnetic resonance field responses, (i) large magnetic response at the center of SRR and (ii) strong electric field localization at the SRR gap. The magnetic resonance wavelength is red-shifted by $\Delta\lambda_2$ = 100 nm as the VO_2 changes

#115088 - $15.00 USD Received 11 Aug 2009; revised 17 Sep 2009; accepted 18 Sep 2009; published 25 Sep 2009

phase from insulator to metal. Introducing nanowires as an additional element to the metamaterial unit cell resulted in narrower resonance peaks than those observed for ordinary SRR arrays. The FWHM of the resonance peaks at 1.8 and 3.0 μm were measured to be 0.5 and 0.7 μm, respectively. The FOM of ordinary SRR array was 0.08, whereas the FOM for the nanowire coupled SRRs is 0.14, due to the spectral line-width narrowing of the metamaterial resonance.

Breaking the structural symmetry of metamaterials has been shown to yield narrower metamaterial resonances at microwave frequencies [28]. Coupling a nanowire to a single SRR is a way to introduce asymmetry to the resonant elements. Another approach is to couple two SRRs of different sizes (asymmetric SRRs) by properly designing the unit cell. Figure 4b shows the reflection spectra of two face-to-face SRRs of different dimensions (Fig. 1c) in the insulator and metallic phases. The resonant peaks for these SRRs are $\lambda_1 = 2.1$ μm and $\lambda_2 = 3.1$ μm. Simulated field plots (inset) show the signal at λ_1 is due to resonances in both SRRs, whereas the signal at λ_2 is due only to the SRR with longer arms. In the case of coupled SRR arrays, the shorter wavelength response is due to the SRR with shorter arms. The total shift upon phase change in the VO_2 is $\Delta\lambda_2 = 110$ nm. Figure 4c shows the reflection spectra for an array of back-to-back coupled SRRs (Fig. 1d) with the same dimensions as the face-to-face structures. Coupling the SRRs in this manner narrowed the wavelength separation of the two resonant peaks: λ_1 red shifted by 200 nm to 2.3 μm and λ_2 blue shifted by 300 nm to 2.8 μm. The change in the magnetic resonant reflection peaks for these coupled structures is $\Delta\lambda_1 = \Delta\lambda_2 = 65$ nm. We observed the hybridization of the resonant wavelength of a single SRR, $\lambda = 2.52$ μm, to shorter and longer wavelengths, λ_1 and λ_2. Different coupling schemes resulted in different peak positions in the reflection spectra. The resonant peak shift depends on the coupling strength of resonator elements, and in the case of strong coupling, resonant peaks show larger shifts [29]. Since the electric fields are strongly localized at the gap of SRRs, the coupling of face-to-face SRRs is stronger than back-to-back coupled SRRs. We observed larger resonance wavelength separation in the case of face-to-face SRRs.

3. Summary

Metamaterial resonances can be engineered using different coupling and hybridization mechanisms as reported here. The three geometries investigated here show reflection resonances of different magnitudes, at wavelengths dependant on the size and degree of coupling between SRRs. In all cases, the magnetic resonance reflection peaks of self-aligned structures red shift as the overall geometry changes with the VO_2 insulator-metal phase transition. Here, we proposed a sandwiched VO_2 active layer between an Ag SRR and sapphire substrate, which caused wavelength tuning of ~100 nm. Incorporating VO_2 nanostructures at different resonant metamaterial elements such as the SRR gap or SRR arms by two-step electron-beam lithography and processing could yield better device performances and higher tuning ratios. In this work the phase change was induced thermally simply by heating the metamaterial array, but optical and electrical phase changes are also possible in VO_2.

In conclusion, we have demonstrated the first active metamaterial at near-IR wavelengths based on an Ag/VO_2 design allowing us to change the optical geometry of the resonant element with the heat induced phase transition of VO_2. Resonance hybridization with additional coupling elements such as nanowires or different size SRRs led to narrower metamaterial resonant peaks, thus increasing the frequency-tuning figure of merit.

Acknowledgements

We acknowledge financial support from the National Science Foundation under Grant DMR 0606472, and the Army Research Office; portions of this work were performed in facilities sponsored by the Center for Science and Engineering of Materials, and NSF MRSEC. We gratefully acknowledge critical support and infrastructure provided for this work by the Kavli

#115088 - $15.00 USD Received 11 Aug 2009; revised 17 Sep 2009; accepted 18 Sep 2009; published 25 Sep 2009

Nanoscience Institute at Caltech. I. M. P. acknowledges the support of a National Science Foundation Graduate Fellowship. We also gratefully acknowledge the help of Professor George Rossman for IR facilities and measurements.

* These authors contributed equally to this work.

‡ Present address: Booz Allen Hamilton, Arlington VA, 22203.

#115088 - $15.00 USD Received 11 Aug 2009; revised 17 Sep 2009; accepted 18 Sep 2009; published 25 Sep 2009